International Journal of Thermofluids 25 (2025) 100991

Contents lists available at ScienceDirect

International Journal of Thermofluids

journal homepage: www.elsevier.com/locate/ijtf

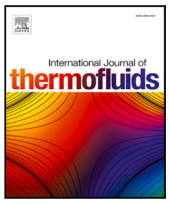

Assessment of an effervescent breakup model for Lagrangian simulations of real fuel sprays

Francesco Duronio [a,c,*], Anqi Zhang [b], Le Zhao [b], Angelo De Vita [a]

[a] Dipartimento di Ingegneria Industriale Informazione e di Economia - Università degli studi dell'Aquila, Piazzale Ernesto Pontieri, Monteluco di Roio, 67100, L'Aquila, Italy

[b] Aramco Americas: Aramco Research Center - Detroit, Novi, 48377, MI, USA

[c] Consiglio Nazionale delle Ricerche, Istituto di Scienze e Tecnologie per l'Energia e la Mobilitá Sostenibili (STEMS), Via G. Marconi 4, Napoli, 80125, Napoli, Italy

ARTICLE INFO

Keywords:
Flash boiling
Effervescent breakup
Real fuel
Lagrangian simulation

ABSTRACT

Flash boiling drastically alters the characteristics of spray atomization and plume structure, which could impose challenges for modern propulsion systems design regarding fuel/air mixture formation and emission performances. Numerical simulations serve as effective tools to understand and predict flash boiling sprays for modern engine applications. This study carried out Eulerian–Lagrangian spray simulation campaigns for two gasoline injectors, and realistic single-composite and multi-component fuel models were used instead of simple surrogates. A validated effervescent breakup model was adopted to account for the non-trivial breakup mechanism induced by bubble nucleation within the liquid droplets. Effects of key model parameters were discussed in detail to propose a consistent set of model constants, and comprehensive validation was achieved against near- and far-field spray experiments. The effervescent breakup model has demonstrated satisfactory effectiveness, and the numerical findings also highlight the necessity of employing real fuel properties for spray analysis.

1. Introduction

Under part load operation of modern gasoline engines, the direct injection of the evaporative fuel into engines' combustion chambers often results in an instantaneous phase transition phenomenon known as flash boiling [1,2].

Flash boiling sprays develop when pressurized liquid expands into ambient environment below its saturation pressure. During this process, the liquid experiences breakup together with strong evaporation, where bubbles could form inside liquid cores and contribute to enhanced atomization of the spray. Liquid atomization by means of the flash boiling mechanism could be a promising method to generate high-quality spray characterized by small droplets across a narrow size distribution [3–9].

Meanwhile, flash boiling sprays could also introduce a significant counter effect when the fuel jets are discharged from multi-hole injectors and collapse [3,10,11]. Under such circumstance, these issued jets deflect towards each other and merge into a single jet, potentially resulting in undesirable spray-wall impingement [5,6].

Understanding the flash boiling spray collapse phenomenon is crucial for optimizing air/fuel mixture quality and ultimately enhancing combustion efficiency for engine applications. Extensive Computational Fluid Dynamics (CFD) research has been conducted to comprehend the physics of spray collapse. Studies utilizing Eulerian–Eulerian (E–E) codes with specific phase transition models could provide great spray details at elevated computational cost. These studies reveal complex mechanisms involving under-expanded jets, air entrainment, and the creation of low-pressure zones, which all emerge as primary contributors for spray collapse [12–14]. On the other hand, the Eulerian–Lagrangian (E–L) approach stands out as an efficient solution for simulating liquid sprays with reduced computational demands, which could be practically integrated into full engine simulations for industry applications [15]. However this approach has some limitations which are mainly related to the fact that they rely on a series of empirical sub-models that lack of a correct physical interpretation of the phenomena and whose parameters need to be tuned to match experimental data. The E–E could assist on setting up E–L simulations but the computational resources need are relevant and often not affordable.

Within the E–L framework, the breakup model is crucial because it strongly influences the droplets sizing which, in turn, affects the dynamics of the mixture formation process. Traditional models such as Kelvin Helmholtz–Rayleigh Taylor (KH–RT) or Reitz–Diwakar (RD) consider the breakup as a consequence of aerodynamic instabilities

* Corresponding author.
E-mail address: francesco.duronio@univaq.it (F. Duronio).

https://doi.org/10.1016/j.ijft.2024.100991
Received 10 May 2024; Received in revised form 10 September 2024; Accepted 28 November 2024
Available online 4 December 2024

Table 1
Lagrangian framework physical sub-models.

Injection model	Blob
Effervescent breakup	fbBreakup
Aerodynamic breakup	Reitz–Diwakar
Heat transfer	Ranz–Marshall
Vaporization	Flash Boiling Vaporization
Collision	No Time Counter (NTC)
Coalescence	Post and Abraham
Dispersion	O'Rourke

that grow on the droplet surface. However, the aerodynamic breakup model constants often require quite extreme tuning when describing super-heated flash boiling sprays, which also makes the model configuration incompatible with normal evaporative conditions [16,17]. Such inconsistency could well indicate that aerodynamic breakup alone is insufficient for modeling flash boiling sprays.

To remedy such modeling challenge, an effervescent breakup model, which was specifically designed for flash boiling conditions accounting for the growth of blobs within droplets [18], has been developed and shown significant improvements in achieving realistic spray morphology and droplet sizing results. This effervescent model needs to be considered as an additional primary breakup mechanism working in conjunction with the aerodynamic approach to address the droplet shattering due to thermodynamic non-equilibrium conditions. It must be pointed out that this class of models, unless always involves an atomization process triggered by vapor bubbles dispersed in the liquid, is intended to be used in Lagrangian spray simulations and so it is different from the effervescent atomization devices proposed in other works [19–21]. Various flash boiling models can be found in literature [22–26] but, as far as the authors known, only few examples of implementations in E–L codes of effervescent breakup models can be retrieved. Researchers performed many investigations with E–E approaches [3,10,27,28] using various finite volume CFD codes. Xi X. et al. developed a model for single droplet dynamics [29]. Price et al. developed a zero dimensional model for in-nozzle flash boiling [30, 31]. On the opposite, many scientific studies can be found regarding experimental observation of flash boiling sprays [32–34]

Leveraging existing technical developments, this work aims to demonstrate an improved modeling framework using Eulerian-Lagrangian simulations for real fuel sprays under flash boiling conditions. As customary, the liquid droplets are modeled as Lagrangian parcels while, the gaseous/vapor phase, is treated with a finite volume approach. The framework adopted incorporates the aforementioned effervescent breakup model and an enhanced phase transition model, and detailed model calibration has been performed to ensure validity. In addition, newly-developed fuel models representative of real fuel physical properties are adopted in this analysis to highlight the distinct spray behavior compared to simple surrogate inputs, which further demonstrates the realistic value of the proposed methodology. More details of the procedure we elaborated are reported in the next.

Two numerical campaigns were performed throughout this investigation. The first campaign focused on the near-nozzle spray behavior through a 6-hole side mounted injector, where comprehensive sensitivity studies were performed to validate the numerical results. The calibrated model was then applied to the second numerical campaign which verified the far-field spray morphology against fuel spray measurements from an 8-hole centrally mounted injector. The paper is structured into six sections: after this introduction, the mathematical and numerical methods, and in particular the breakup model, are presented. Then, the two investigated case studies are discussed in sequence to highlight detailed model features and their effectiveness. Lastly, the concluding remarks summarizes key learning from this model development practice.

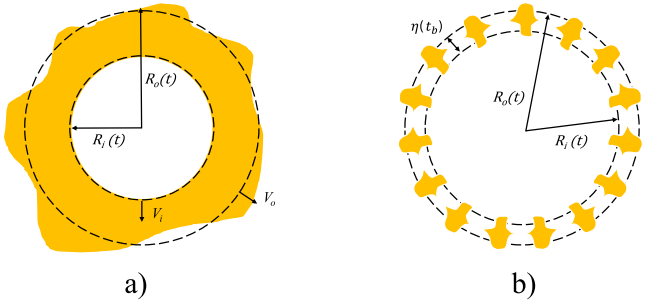

Fig. 1. Time evolution of bubble–droplet system [18].

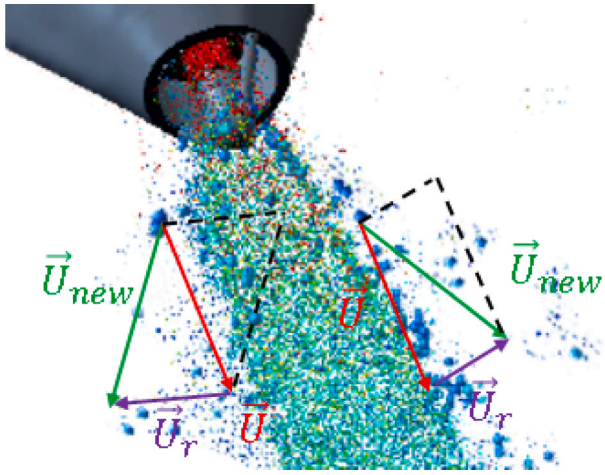

Fig. 2. Droplet velocity after breakup updating [15].

2. Mathematical and numerical methods

The simulations were performed using a modified PISO algorithm to solve the finite volume problem, and the discrete droplet method (DDM) was adopted for the Lagrangian framework solution [35]. Turbulence was modeled using the RNG k-ϵ RANS setup, which is common for internal combustion engine simulations [16,36]. Table 1 documents major physical sub-models adopted in this work.

Most sub-model selections are typical for Lagrangian spray simulations [37–39], while specific modeling treatments were applied to the *breakup* and *phase-change* sub-models to account for the flash boiling conditions of interest. These specific model details are discussed below.

2.1. Effervescent breakup: bubble formation

During the flash boiling process, the growth of bubbles within the super-heated droplets gives rise to a thermodynamic breakup mechanism that operates approximately one order of magnitude faster than the conventional aerodynamic breakup. [41,42]. The **fbBreakup** model was previously developed by the authors to describe the effervescent breakup process resulting from the flash boiling sprays [18], and has been implemented as a user defined function (UDF) within CONVERGE 3.0 CFD code [38] for this study.

Fig. 1 illustrates the main hypothesis of the effervescent breakup using the bubble–droplet system. In essence, when the liquid is injected under super-heated conditions, vapor bubbles nucleate within the liquid sheets [31]. Their initial radius, $R_{i,0}$, arises from the equilibrium between the liquid surface tension (σ) and the pressure forces inside the bubble–droplet system, as described by Eq. (1)

$$R_{i,0} = \frac{2\sigma}{P_{sat}(T_0) - P_\infty} \tag{1}$$

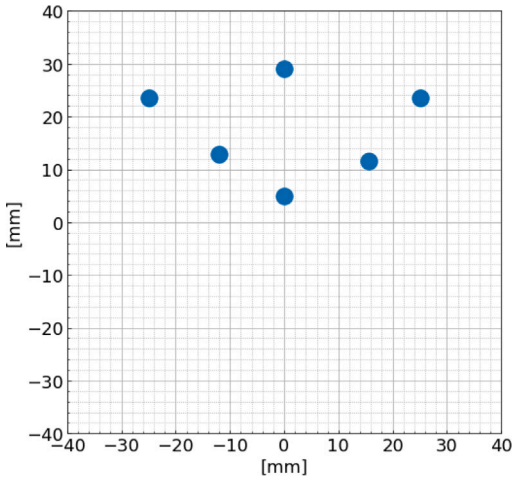

Fig. 3. Spray targets of the side mounted 6-hole injector.

where P_{sat} is the liquid saturation pressure and P_{∞} is the ambient pressure computed in the Eulerian framework. If the vapor bubbles have a radius smaller than $R_{i,0}$, they collapse under the force of the surface tension. Any variation of the pressure difference "$P_{sat}(T_0) - P_{\infty}$" will cause the bubble to grow or collapse, and for this reason, it is also considered the critical radius of the vapor bubbles.

In this model, the bubble growth rate (V_i) is computed using a simplified Rayleigh–Plesset equation, where secondary terms are considered negligible under the assumption of inertial-dominated growth. This assumption is justified because, for a bubble growing in a superheated droplet, the timescales from initiation to droplet breakup are on the order of tens of microseconds, which are much faster than vaporization and heat exchange phenomena [43].

$$V_i = k_{Vb}\sqrt{\frac{3}{\rho_l}\left(p_{sat} - p_{\infty}\right)} \tag{2}$$

The first **fbBreakup** model constant, k_{Vb}, is introduced as the bubble growth rate constant as shown in Eq. (2). Consequently, the droplet growth rate (V_o) can be expressed as a function of the bubble growth rate [42]:

$$V_o = V_i \cdot \Delta^2 \tag{3}$$

where $\Delta = \frac{R_o}{R_i}$.

2.2. Effervescent breakup: breakup criterion

Effervescent breakup is due to the instabilities that grow along the droplet and bubble surfaces (Fig. 1-a). The instability growth rate ω is the largest real root of the following normalized growth rate equation [42]:

$$\left(\Delta - \Delta^2 - \psi_o\Delta\right)\Omega^2 + \left(-1 + \Delta^4 + \psi_o\right)We_o^{1/2}\Omega + 2\Delta^2 + 2\Delta^{-2} - 3\psi_i\frac{We_i}{Ma_i^2}\frac{\Omega}{\Omega+3\,We_i^{1/2}}\Delta^2 = 0 \tag{4}$$

where:

$$\Omega = \sqrt{\frac{\rho_\ell R_i^3}{\sigma}}\omega, \quad We_o = \frac{\rho_\ell V_o^2 R_i}{\sigma}, \quad We_i = \frac{\rho_\ell V_i^2 R_i}{\sigma}, \quad Ma_i = \frac{V_i}{c}, \quad \Delta = \frac{R_o}{R_i}, \quad \psi_o = \frac{\rho_{go}}{\rho_\ell}, \quad \psi_i = \frac{\rho_{gi}}{\rho_\ell} \tag{5}$$

V_i and V_o are the bubble and droplet growth rate previously introduced, while ρ_{go} and ρ_{gi} are the gas densities inside and outside the bubble–droplet system. The temporal evolution of this instability, denoted as η, growing with the rate ω, is given by the following relation:

$$\ln\left(\frac{\eta}{\eta_0}\right) = \int_0^t \omega dt \tag{6}$$

When the instability amplitude becomes larger than a characteristic length of the spray (Fig. 1b) [44], typically chosen as the liquid thickness of the bubble–droplet system (i.e., the difference between droplet and bubble radius $R_o(t) - R_i(t)$), breakup takes place. Assuming the initial disturbance η_0 is proportional to the initial droplet radius, $\eta_0 = 0.05 \cdot R_o\left(t_0\right)$, a breakup criterion, for bubble–droplet systems under thermal non-equilibrium, can be expressed as:

$$\eta_0 e^{\int_0^t \omega dt} = k_b[R_o(t) - R_i(t)] \tag{7}$$

where k_b is the second **fbBreakup** model constant which addresses the complexities inherent in bubble–droplet systems.

2.3. Effervescent breakup: post-breakup behavior

The present effervescent breakup is catastrophic and results in droplet explosion, plume expansions, and subsequent plume-to-plume interactions, as broadly observed through experiments. To reproduce this behavior, once the breakup occurs, a radial velocity component is introduced to the broken-up droplets, as shown in Fig. 2.

The magnitude of the radial velocity $\left(U_r\right)$ can be computed applying mass and momentum conservation before and after breakup [42]:

$$U_r = k_v\frac{3R_i^2V_i\left(R_o - R_i\right)}{R_o^3 - R_i^3} \tag{8}$$

where k_v is introduced as the third **fbBreakup** model constant to account for the spray expansion magnitude. The orientation of U_r is randomized over a plane perpendicular to the parcel velocity vector prior to the breakup occurrence. As a result, the new droplet acquires further velocity components:

$$U_x = U_{x,old} + U_{xr} \quad U_y = U_{y,old} + U_{yr} \quad U_z = U_{z,old} + U_{zr} \tag{9}$$

The Sauter mean radius (SMR_{32}) of the new droplets can be obtained through the following relation derived from the conservation of mass and energy [42]:

$$SMR_{32}^{-1} = \frac{1}{2}\frac{R_0^2 + R_i^2}{R_o^3 - R_i^3} + \left(\frac{3}{2}\frac{R_i^4\left(R_i^{-1} - R_o^{-1}\right)}{R_o^3 - R_i^3}V_i^2 - \frac{U_r^2}{2}\right)\frac{\rho_\ell}{3\sigma} \tag{10}$$

And the number of new droplets n_{new} can thus be updated following mass conservation:

$$n_{new}d_{new}^3 = n_{old}d_{old}^3 \tag{11}$$

where n_{old} is the number of particles prior to the breakup process.

2.4. Aerodynamic breakup

Even under flash boiling conditions, the aerodynamic breakup is still a major liquid breakup mechanism and needs to be properly modeled. In this study, the Reitz–Diwakar model [31,36] was developed within CONVERGE and adopted to account for aerodynamic breakup. Throughout one simulation, each parcel undergoes the effervescent breakup only once, while the aerodynamic breakup can be applied multiple times to a single parcel. The **fbBreakup** model has been implemented with physics-based criteria to adaptively identify flash boiling conditions. This combined effervescent/aerodynamic breakup treatment has shown effectiveness through prior work [18,41].

2.5. Droplet evaporation

In addition to introducing the effervescent breakup mechanism, flash boiling strongly influences the phase change process. The Price model was adopted for describing super-heated liquid phase transition [30]. The combined droplet evaporation sub-model accounts for

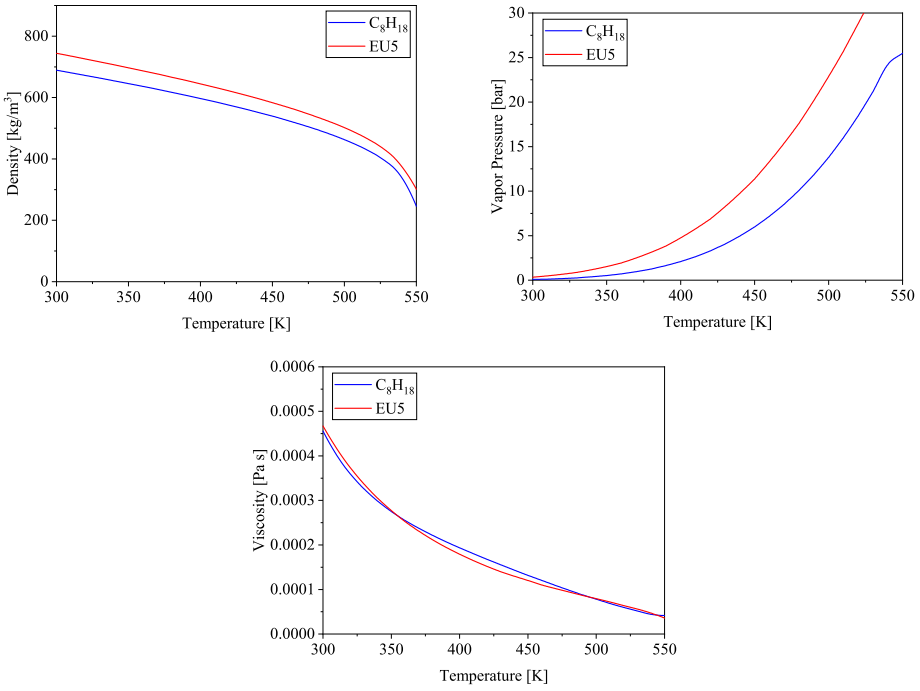

Fig. 4. Comparison of physical properties of iso-octane and EU5 fuel model.

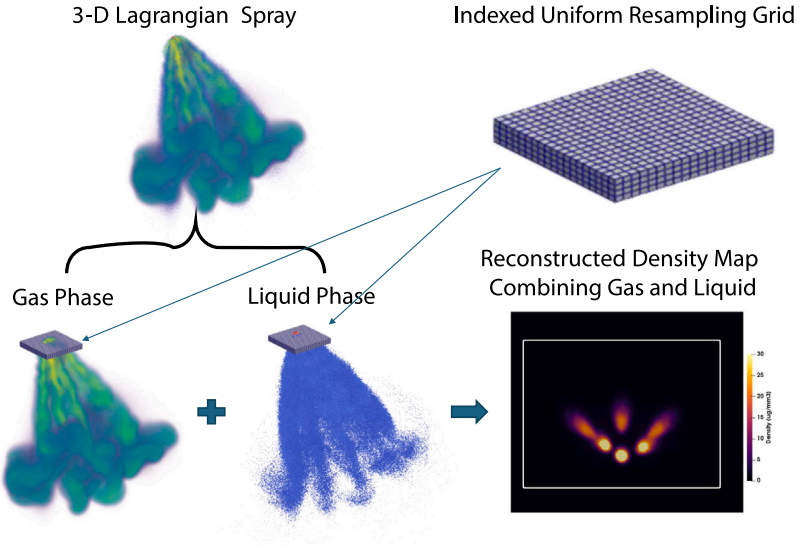

Fig. 5. Overview of the post processing approach developed to compare Eulerian–Lagrangian simulations with x-ray measurements.

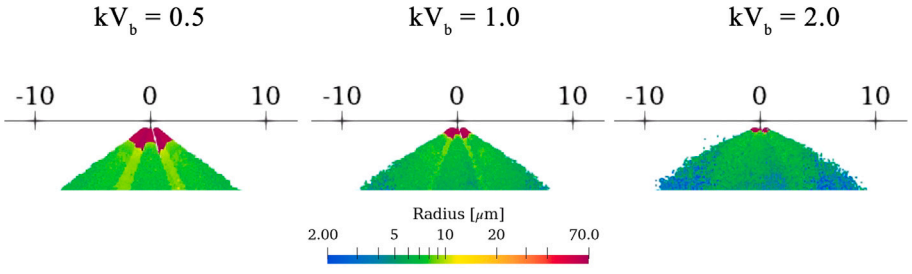

Fig. 6. Near-nozzle spray morphology at 1 ms after the SOI with different k_{Vb} values. (For interpretation of the references to color in this figure legend, the reader is referred to the web version of this article.)

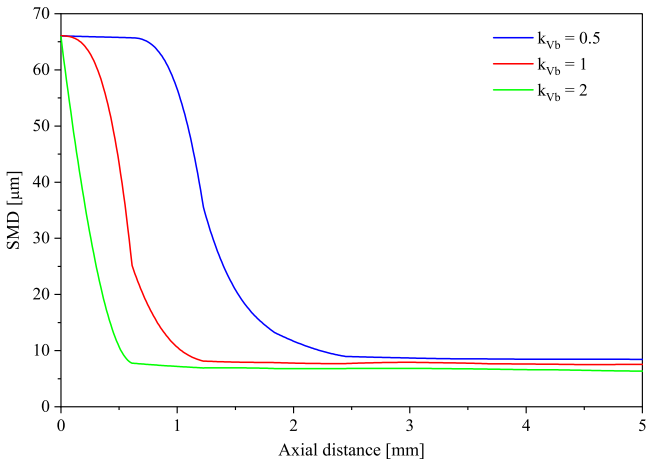

Fig. 7. Near-nozzle spray SMD at 1 ms after the SOI with different k_{Vb} values.

both sub-cooled and super-heated contributions to the droplet evaporation. The sub-cooled term M_{SC} is computed using the following equation:

$$\frac{dM_{SC}}{dt} = 2\pi R P_\infty \frac{Sh D_i}{T_f R_f} \ln\left(\frac{P_\infty - P_v}{P_\infty - P_S}\right) \tag{12}$$

where:

- R is the drop radius;
- P_∞ is the ambient pressure;
- Sh is the non-dimensional Sherwood number, function of Reynolds and Schmidt number: $Sh = 2 + 0.6Re^{0.5}Sc^{0.33}$
- D_i is the binary diffusivity coefficient;
- T_f is the vapor film temperature (the average of the droplet and the surrounding gas temperatures);
- R_f is the vapor film specific gas constant;
- P_v is the partial vapor pressure of the drop species;
- P_{sat} is the saturation pressure of the species.

And the super-heated term M_{SH} is:

$$\frac{dM_{SH}}{dt} = \frac{4\pi R^2 \alpha \left(T_d - T_b\right)}{H_L} \tag{13}$$

where:

- H_L is the latent heat of the liquid;
- T_b is the boiling temperature of the fuel at the specific ambient pressure;
- T_d is the instantaneous droplet temperature;
- α is a heat transfer empirical coefficient, whose values can be found in [31].

Subsequently, the total evaporation rate is:

$$\frac{dM_t}{dt} = \frac{dM_{SC}}{dt} + \frac{dM_{SH}}{dt} \tag{14}$$

3. First campaign: 6-Hole side mounted injector

3.1. Experimental and numerical setup

3.1.1. Material information

The investigated spray is formed by a solenoid-actuated GDI injector, featuring 6 counter-bored spray orifices in a side mounted configuration. The center of the spray plume is orientated at an angle with respect to the injector axis, and the specific orientation of each individual orifice is depicted by the spray footprint at 30 mm shown in Fig. 3. The sizes of the counter-bore and nozzle orifices are equal to 153 ± 8 μm and 296 ± 2 μm, respectively [45]. The investigated conditions are summarized in Table 2.

Table 2
Investigated operating conditions.

Injection pressure [bar]	50
Ambient pressure [bar]	0.4
Ambient temperature [K]	298
Fuel temperature [K]	363
Fuel injected	EU5 cert. gasoline/iso-octane
Injected quantity [mg]	11.65
Injection duration [ms]	2.0

The morphology of flash boiling sprays could be affected by the liquid properties of the injected fuel. Real gasoline fuels are typically complex mixtures of hundreds of hydrocarbons and challenging to model. A few methods have been developed to represent the complex real fuels in numerical analysis, as listed in 3. As the fuel model becomes more accurate and representative, the model complexity and computational cost also increases.

The first campaign adopts a single-composite fuel model for a sample of Euro 5 certification gasoline (EU5) based on its Detailed Hydrocarbon Analysis (DHA). A numerical process adopting Aspen HYSYS was then used to calculate the averaged properties of DHA-identified chemical compounds. These averaged properties were tabulated against temperature and pressure to be used for 3-D CFD simulations. Fig. 4 provides a liquid property comparison between the single-composite fuel model and iso-octane, a commonly used simple fuel surrogate. While both candidates share similar liquid density and viscosity, the single-composite fuel model appears more volatile with generally higher vapor pressures than iso-octane.

3.1.2. Numerical setup

The Lagrangian sprays were simulated in a cylindrical domain of 100 mm diameter and 85 mm height filled with nitrogen to ensure the free development of the spray. The boundaries of the domain are considered as adiabatic walls. CONVERGE CFD code handles the geometry discretization [38,46] and creates base grids of 2 mm in each direction. Fixed embedding refinement was applied in the near-nozzle zone, and adaptive mesh refinement (AMR) was enabled based on the velocity gradient. A base mesh refinement strategy was applied with 3 levels of fixed embedding (0.125 mm minimum near-nozzle grid size) and 2 levels of AMR (0.25 mm far-field grid size), which is typical for similar fuel spray simulations.

The blob injection model initialized liquid parcels during the simulation with droplet size matching the nozzle diameter. C_d coefficient is equal to 0.7385 and C_v to 0.7385. The spray plume cone angles were obtained from injector manufacturer specification. The number of parcels injected was chosen accordingly with the grid dimensions as suggested in [38,47]. The aerodynamic breakup model constants C_{bag}, C_b, C_{strip} and C_s used in the Reitz–Diwakar model are specified in Table 4 and kept unchanged in this paper.

3.1.3. Post-processing method

Since the near-nozzle density distribution obtained through tomographic reconstruction of X-ray radiography [48] was used for validation, it is essential to properly post-process the simulation output to ensure meaningful comparison and analysis. The non-trivial aspect of the procedure is to processes both the Lagrangian liquid phase and Eulerian vapor phase, as the near-nozzle vapor mass is not likely negligible when flash boiling occurs. As shown in Fig. 5, an indexed uniform resampling grid was setup to resample the near-nozzle vapor and liquid fields. With the grid index information, both the liquid and vapor mass could be attributed to the corresponding spatial grid, which allows for density distribution calculation with known volumes of the grids. Subsequently, a slice through the resampled density field could be extracted to be compared with experiment measurements.

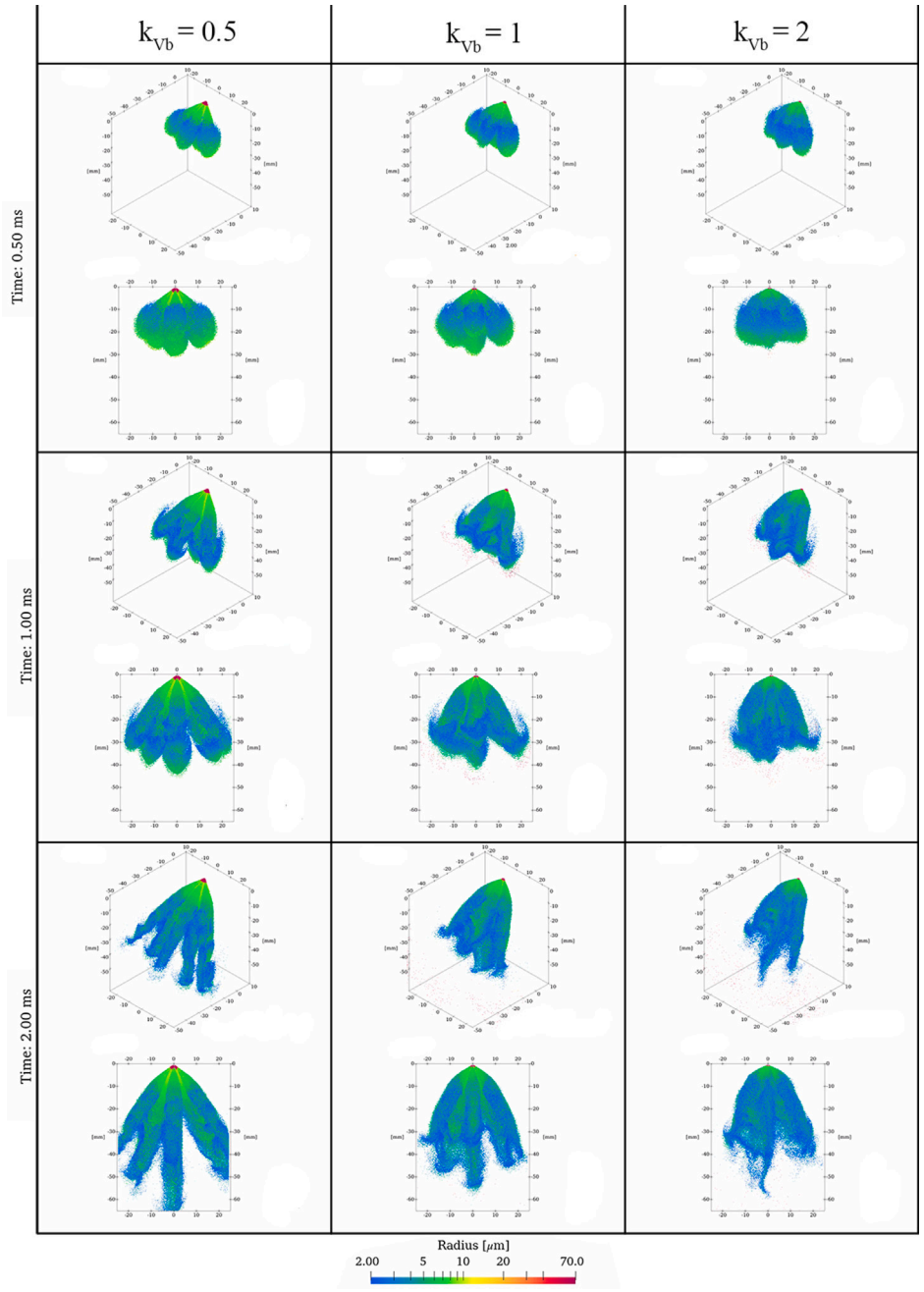

Fig. 8. Sensibility study for the parameter k_{Vb}. Overview of the morphology of the spray at different temporal instants.

Table 3
Analytical methods to represent real fuels.

	Method	Species count	Representing average liquid property	Representing distillation behavior
1	Simple surrogate (e.g. iso-octane)	1	No	No
2	Single-composite fuel model	1	Yes	No
3	Multi-component fuel model	O(10)	Yes	Yes

Table 4
Breakup model parameters.

C_{bag}	6
C_b	1.5
C_{strip}	1
C_s	10

3.2. Results and discussion

Under this section, the effects of each individual model constant are first studied, which leads to the best practice proposal of these model constants. The best practices are then examined for grid convergence and fuel property effects.

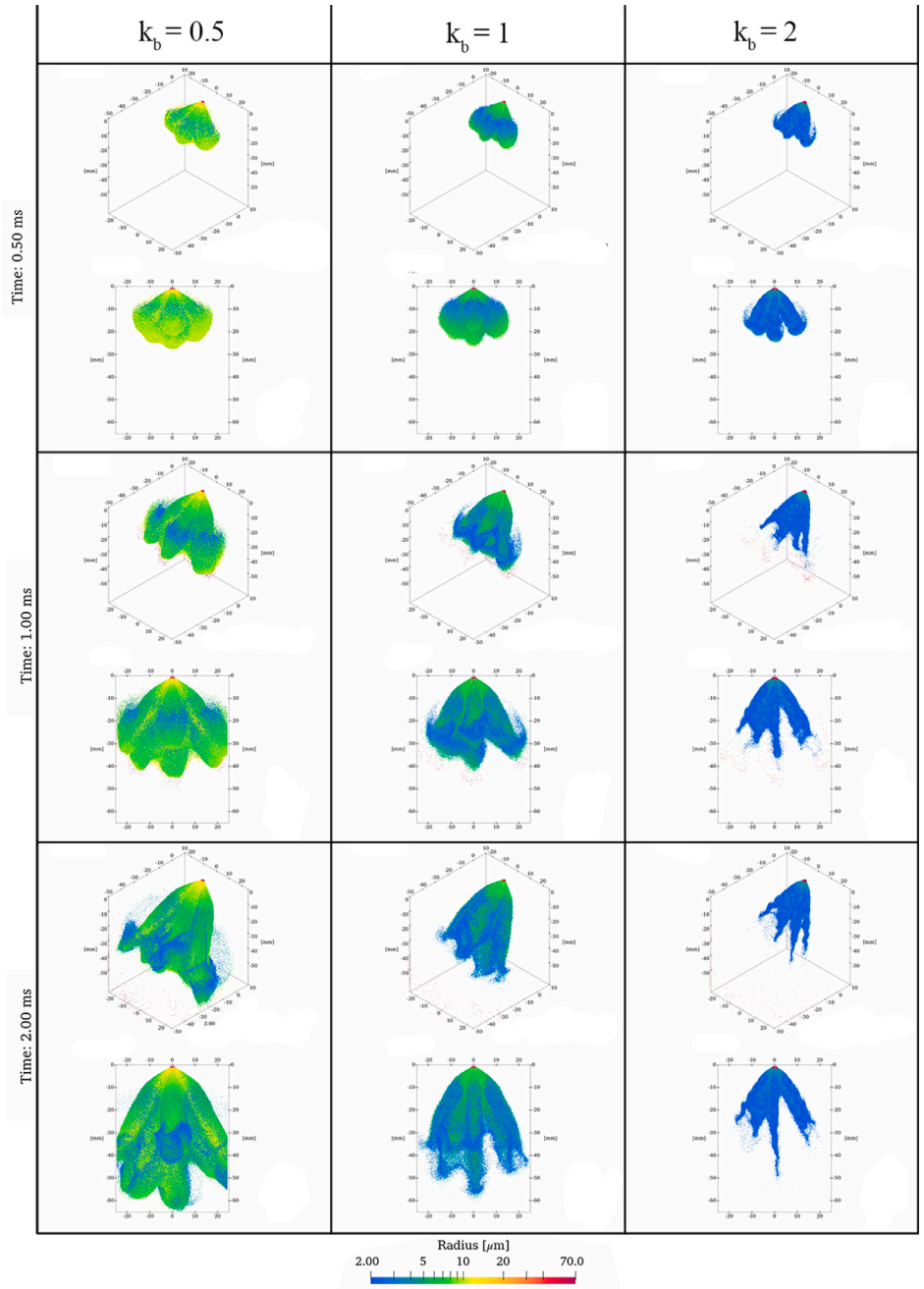

Fig. 9. Sensibility study for the parameter k_b. Overview of the morphology of the spray at different temporal instants. (For interpretation of the references to color in this figure legend, the reader is referred to the web version of this article.)

3.2.1. *Effect of k_{Vb}: bubble growth rate constant*

The sensitivity analysis on the parameter k_{Vb} is reported in Figs. 6–8. The k_{Vb} value varied from 0.5 to 2, while the other two model constants were held at unity. As the k_{Vb} value increases, the unbroken zone denoted by dark red colors in Fig. 6 becomes shorter, indicating accelerated atomization. Fig. 7 quantify this aspect reporting the SMD plotted as a function of the axial distance for the three values of k_{Vb} investigated at 1 ms after the SOI. The faster bubble growth driven by large k_{Vb} values causes the initial droplets to breakup earlier and forms small-sized droplets closer to the injector tip as depicted by the blue colors in Fig. 6 for the $k_{Vb} = 2$ results. The effect of changes in the spray development is depicted in Fig. 8 which reports the same temporal instants of Fig. 6 (1 ms after the SOI).

The liquid phase of the sprays, represented by droplet radius, are depicted from two different views in Fig. 8. Increasing k_{Vb} induces an evident spray collapse as shown by the far-field spray morphology. The early breakup with $k_{Vb} = 2$ generated smaller droplets with reduced momentum, which causes the plume trajectories bent towards each other. In addition, with faster bubble growth, the droplet also registered smaller dimensions in the far field and evaporated faster to form slightly shorter penetration.

3.2.2. *Effect of k_b: effervescent breakup criterion constant*

The parameter k_b is the constant that controls the breakup criterion and specifies the required fraction of the characteristic length of the spray initiating breakup. Fig. 9 reports the analysis with k_b values ranging from 0.5 to 2.

As can be observed, k_b could significantly affect the droplet sizes within the spray. This can be depicted also from Fig. 10 that shows the average SMD plotted over time.

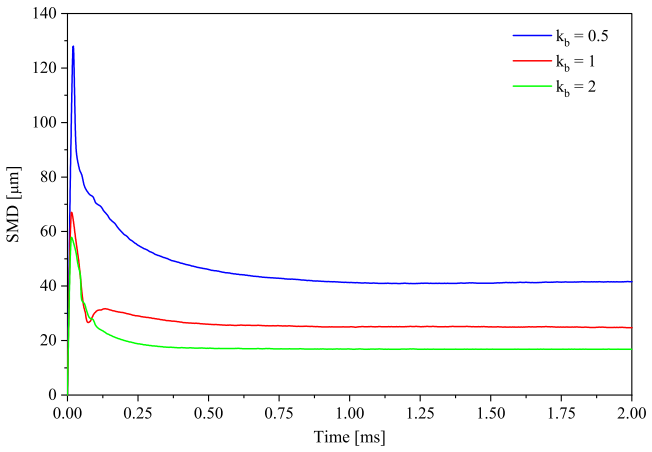

Fig. 10. Sensibility study for the parameter k_b. SMD vs. time after start of the injection.

An obvious droplet size reduction trend could be identified as k_b increases, which was highlighted by the increased fraction of blue color droplets in Fig. 9 for $k_b = 2$. As a result, the absence of large droplets further promoted evaporation and reduced overall liquid penetration. Meanwhile, it should be noted that this k_b parameter has relatively minor effect on the spray shape. Despite the droplet sizing difference, the plumes largely maintained their orientation throughout the injection event.

3.2.3. Effect of k_v: radial velocity constant

The k_v parameter of the **fbBreakup** model, which modifies the magnitude of the radial velocity added after the breakup, is analyzed in Fig. 11. It can be observed that increasing k_v enhances the plume-to-plume interaction, and evident spray collapsing could be observed with $k_v = 2$. The magnified post-breakup velocity component increased the propensity of droplet collision and coalescence from adjacent plumes, resulting in this characteristic feature of flashing sprays. Although very effective in promoting spray collapsing, this radial velocity constant has shown insignificant effect on droplet sizing or overall spray penetration.

3.2.4. Model constants calibration

An attempt to obtain proper model constant values has been performed by calibrating the simulation results against high-fidelity near-nozzle X-ray measurements. Fig. 12 reports the post-processed density maps at 1 mm downstream the injector tip in axial direction for the tested k_{Vb}, k_b and k_v variants. These density maps refer to 1 ms after SOI when the sprays reach steady-state condition. Similar to previous spray morphology discussions, larger values of k_{Vb} and k_v help to promote plume-to-plume interaction, making the droplets more dispersed to resemble the characteristics of a flashing spray. Furthermore, the three model parameters all demonstrated monotonic influences on certain spray behavior, which is beneficial for the calibration process. Following these observations, an optimal configuration was identified with the values $k_{Vb} = 3$, $k_b = 2$, and $k_v = 2.5$. Fig. 13 shows a comparison of the steady-state density map obtained with the optimized configuration against experimental data from Sforzo et al. [48].

A satisfactory agreement is shown. The desired plume-to-plume interaction was obtained numerically. It should be reminded that if the effervescent breakup was not modeled properly, the resulting density map likely would present six individual plume footprints. In addition, the simulation results share very comparable density magnitudes as the X-ray values, which provides further model confidence from a quantitative perspective.

Table 5
Description of the different grids adopted for CFD simulations.

	Fixed embedding	Min. Grid near-nozzle	AMR level	Min. Grid far-field
Coarse	2	0.25 mm	2	0.25 mm
Base	3	0.125 mm	2	0.25 mm
Fine	4	0.0625 mm	2	0.25 mm

3.2.5. Grid independence test

Three meshing strategies were practiced to verify grid independence of these simulations, namely coarse, base, and fine as shown in Table 5. The effervescent breakup is more likely to be affected by the near-nozzle mesh resolutions, thus the far-field grid size were kept a bit coarse for all meshing strategies to maintain reasonable computation cost.

Fig. 14 reports the grid sensitivity test results using the optimized setup for the effervescent breakup model. It can be observed that with the coarse grid, plume-to-plume interactions are under-predicted, and extended saturation zones are observed on the density map. On the other hand, once the grid gets enough refinement at or smaller than 0.125 mm, reasonable grid independence can be obtained. The fine mesh could lead to some post-processing artifacts, but the shape, magnitude, and distribution of the density map stay quite close to that of the base mesh results. Further mesh effect results are shown in Fig. 15 where the overall spray is represented. The coarse grid could also give rise to a great amount of unbroken parcels in the far field. In summary, grid resolution of 0.125 mm or smaller is required to resolve the spray pattern that is just 1 mm from the injector tip. Coarser mesh could only allow a few grids between the injector nozzle and the plane of interest, which would be insufficient.

3.2.6. Effect of fuel property

Lastly, a small numerical evaluation was practiced to exemplify the effect of the liquid properties of the injected fuel. Fig. 16 compares the density maps resulting from EU5 gasoline and iso-octane simulation runs with the optimized model constants. The resulting iso-octane spray represent sub-cooled behavior under this gasoline flash boiling condition, which is further verified with the overall spray shape as reported in Fig. 17.

As depicted in Fig. 4, iso-octane has notably lower vapor pressure than EU5 gasoline, making it less volatile under the test conditions and thus more resistant to collapse. It could impose major risks for practical hardware development if unrealistic liquid volatility was employed for analysis and led to such distinct spray behavior prediction discrepancy. Consequently, under or near flash boiling conditions, it is critical to account for realistic liquid fuel properties, especially volatility metrics, for delivering trustworthy analysis results.

4. Second campaign: 8-Hole centrally mounted injector

This section reports the second case study investigated, involving fuel sprays from the ECN Spray M injector operating under flash boiling conditions [40]. With the identified model constants from the first numerical campaign, the proposed modeling framework will be evaluated for both near-nozzle and far-field spray prediction performances.

4.1. Experimental and numerical setup

ECN's Spray M injector is an 8-hole gasoline injector with a central symmetric plume pattern. The plumes direction and cone angle are set exploiting from specific measurement available on the ECN website [40], specifically at 32° and 20°. It should be underlined that the adopted plume angle in this study is consistent with the measured direction of the nozzle hole. All 8 nozzles of the injector share the same diameter of 170 μm. Table 6 depicts ECN's flash boiling test condition,

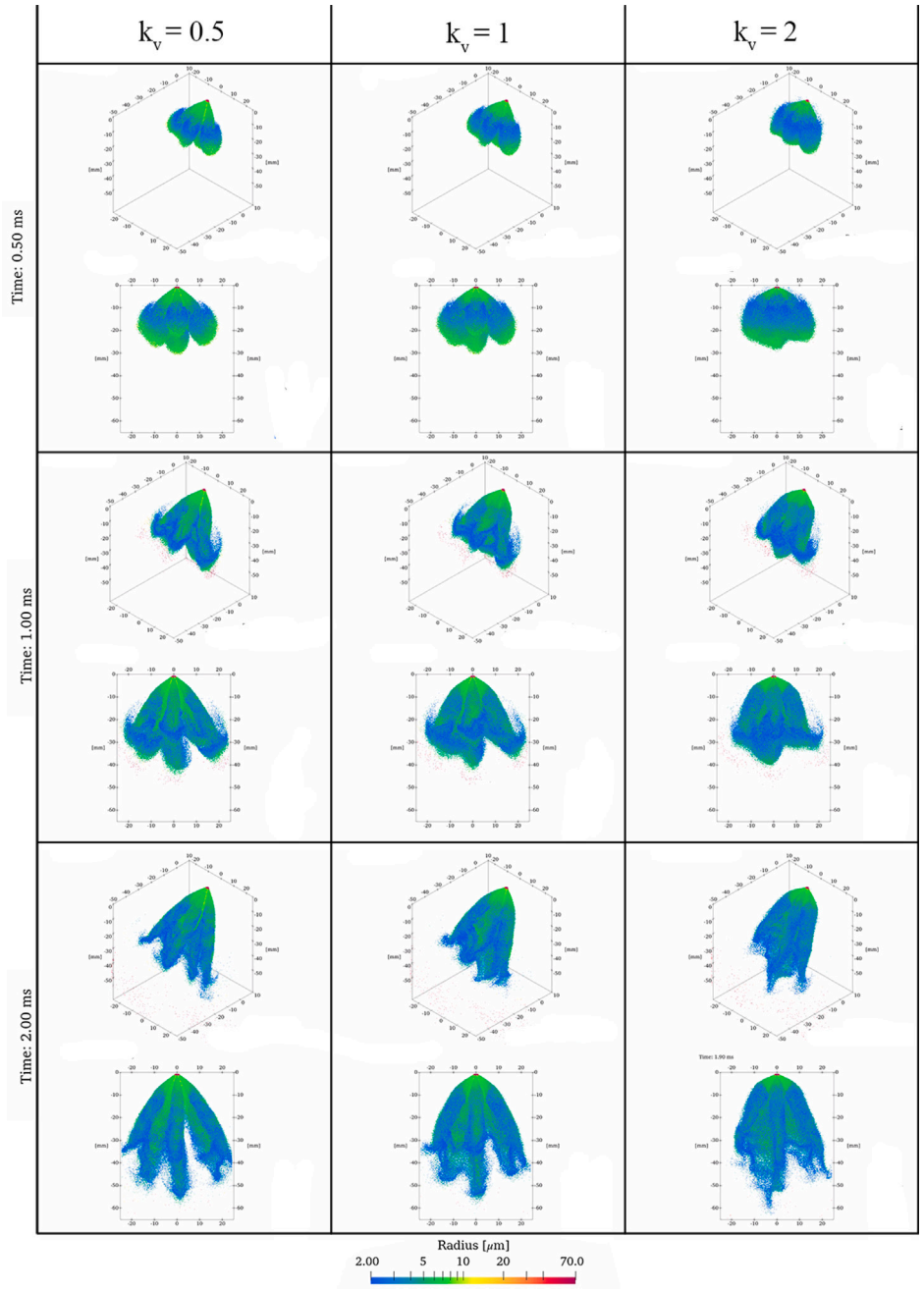

Fig. 11. Sensibility study for the parameter k_v. Overview of the morphology of the spray at different temporal instants.

Table 6
Investigated operating conditions.

Injection pressure [bar]	200
Ambient pressure [bar]	0.5
Ambient temperature [K]	333
Fuel temperature [K]	363
Fuel injected	PACE20

which shares similar ambient pressure and fuel temperature as the first campaign in this paper.

The US DOE's PACE program has spent dedicated efforts to develop the PACE20 fuel model, which is a multi-component fuel model to represent accurate properties of a gasoline fuel [49,50].

This multi-component liquid mixture is comprised of nine different hydrocarbons with specified liquid volume fraction: 0.0955 ethanol, 0.1395 n-Pentane, 0.0541 1-Hexene, 0.0919 Toluene, 0.1153 n-Heptane, 0.2505 Iso-octane, 0.1187 1,2,4-TMB, 0.1050 Cyclopentane, and 0.0295 Tetralin.

The meshing strategy is the same as the previous case: a base grid of 2 mm, near-nozzle refinement to 0.125 mm, and AMR to 0.25 mm throughout the domain. The model constants for effervescent and aerodynamic breakup are kept the same as those identified in the first case study. C_d coefficient is equal to 0.48 and C_v to 0.75.

4.2. Results and discussion

In the following, results from both near-nozzle X-ray measurements and the overall spray development will be illustrated, offering a more

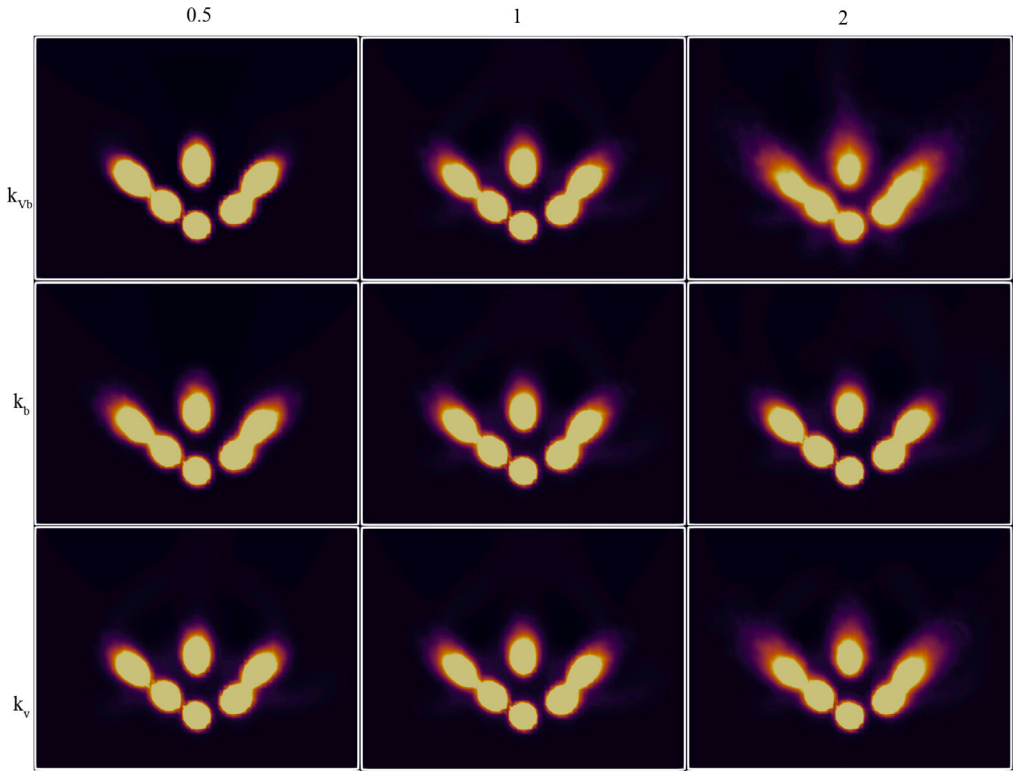

Fig. 12. Spray density maps at 1 mm in axial direction for different values of $k_V b$, k_b and k_v.

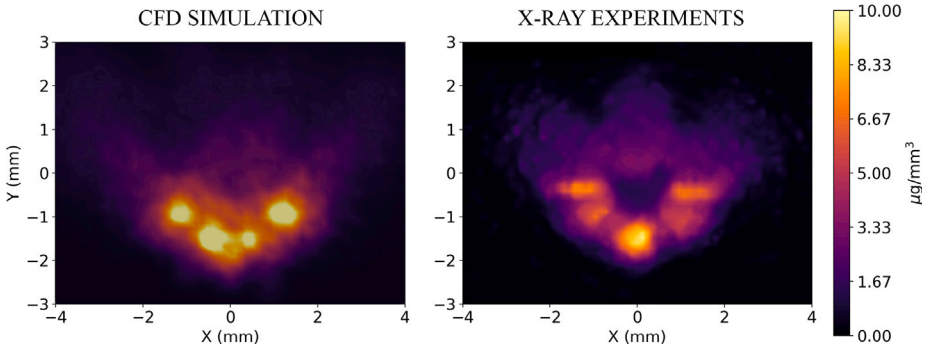

Fig. 13. Spray density maps at 1 mm in axial direction. Comparison of CFD results with X-ray measurements.

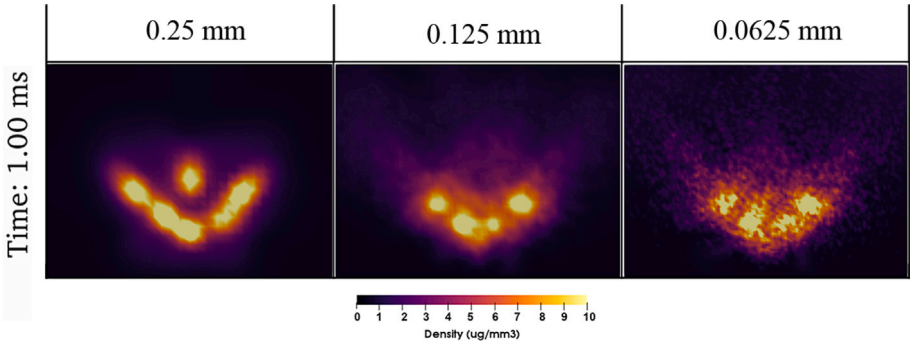

Fig. 14. Spray density maps at 1 mm in axial direction.

comprehensive validation of the effervescent breakup model. Similar to the first campaign, X-ray measurements are used to showcase the capability of the modeling approach to reasonably reproduce the liquid distribution near-nozzle region. As presented in Fig. 18, the moderate plume thickening is well captured by the CFD results with 8 distinguishable footprints. The predicted plume-to-plume interaction appears less evident, potentially due to the neglected differences between the actual plume directions and the geometrical nozzle center line. As illustrated

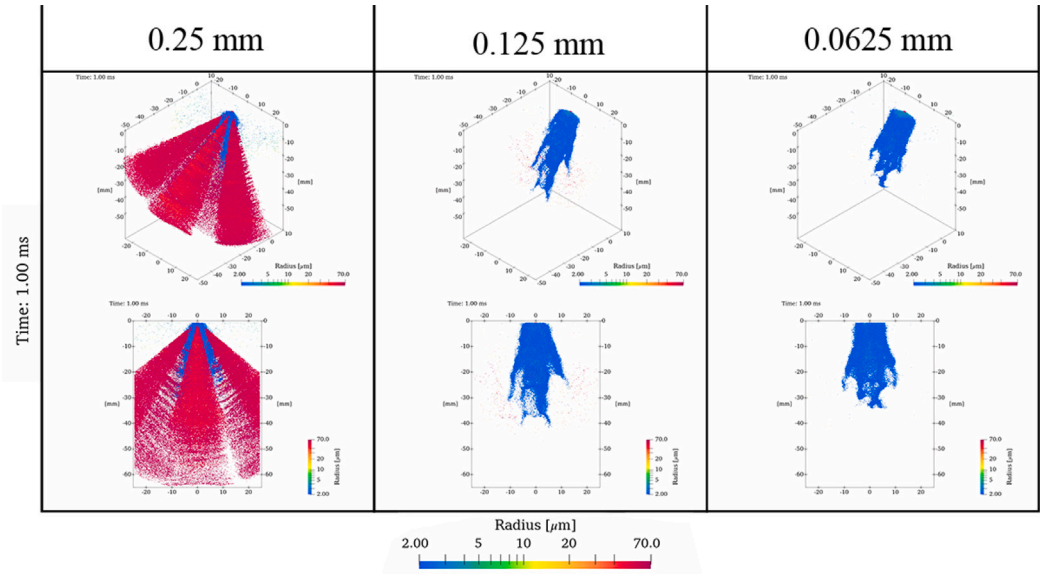

Fig. 15. Spray morphology represented with liquid parcels plotted accordingly with their dimension.

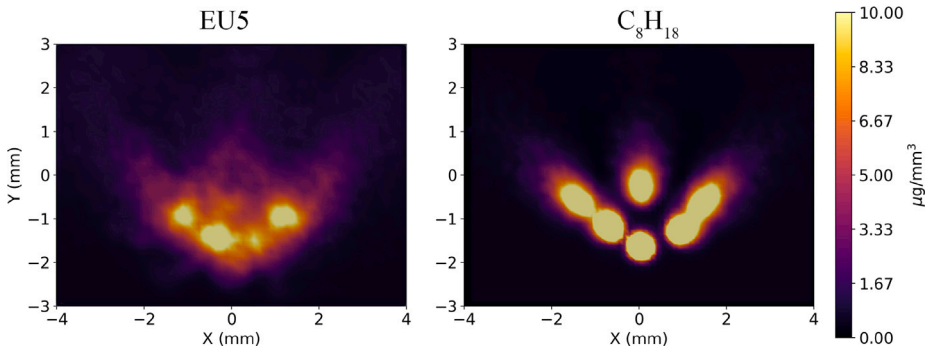

Fig. 16. Spray density maps at 1 mm in axial direction. Comparison of CFD results obtained using EU5 gasoline and iso-octane.

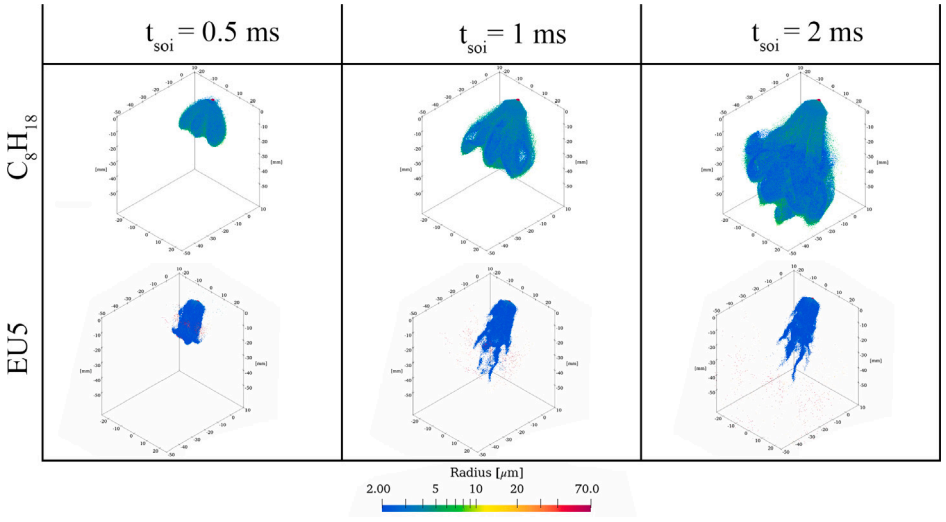

Fig. 17. Spray morphology represented with liquid parcels plotted accordingly with their dimension. Comparison of CFD results obtained using EU5 fuel model and iso-octane.

in [40], the measured plume direction is typically smaller than the drill angle. Fig. 18 reports the experimental and simulated density maps.

In addition, projected liquid volume-fraction (PLV) maps computed from Diffused Back-light Illumination Extinction Imaging (DBIEI) acquisition were used to validate far-field spray predictions. Fig. 19 shows the spray development metrics in terms of liquid penetration and plume width measured at 15 mm from the injector tip. A threshold of $2.0 \cdot 10^{-4}$ $mm^3\ mm^{-2}$ was used to process both experimental and simulated PLV maps for the spray metrics extraction. High-quality agreements between simulation and measurement are observed for not only during

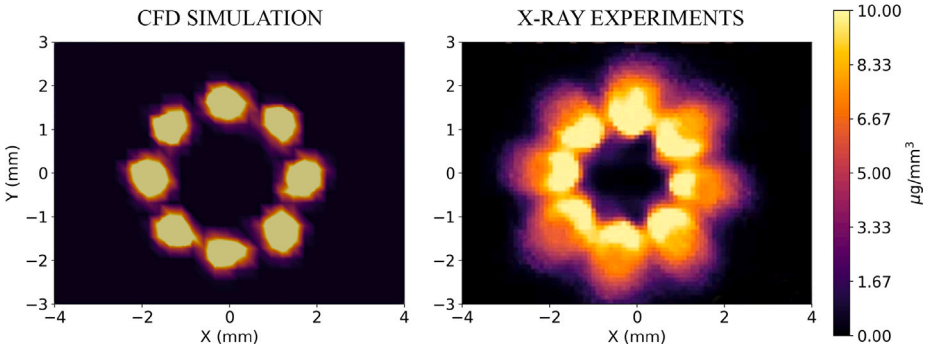

Fig. 18. PACE20 spray density maps at 1 mm in axial direction. Comparison of CFD results with X-ray measurements.

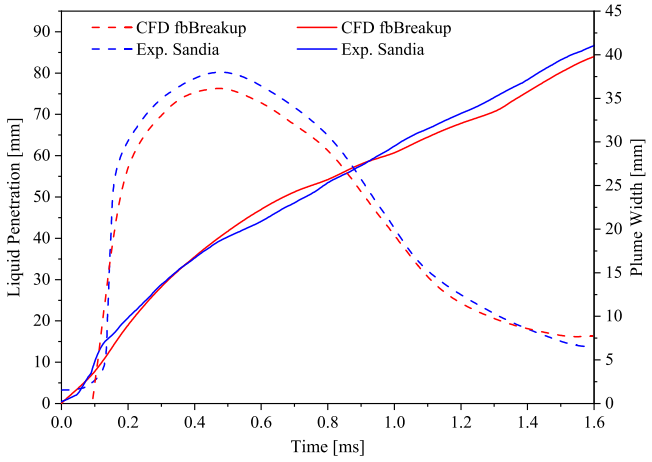

Fig. 19. Numerical vs experimental [40] liquid penetration and plume width for the PACE20 spray.

the injection period but also after the injection ends (after 0.78 ms), justifying strong validation of the spray modeling.

Furthermore, the spray morphology is depicted in Fig. 20 identifying the spray boundaries for two temporal instants. At both 0.6 and 1.2 ms after the start of the injection, the simulated spray shape (blue contour) matches decently with experimental results (black contour). In particular, the spray collapsing is captured using the effervescent breakup model without aggressive altering of other model constants or injector specifications.

The correct representation of the spray collapsing is also evident in Fig. 21, which reports axial sections of the spray taken at a distance of 30 mm from the injector tip at two different temporal instants. Simulation shows similar behavior as the experiments where the peaks of the fuel LVF move towards the axis of symmetry of the spray, highlighting the presence of the collapse. These snapshots clearly demonstrate the **fbBreakup**'s capability on reproducing occurrence of flash boiling.

5. Conclusions

Two Lagrangian simulation campaigns were performed in this study to demonstrate the effectiveness of the novel effervescent breakup model for predicting flash boiling real fuel sprays. The following learning have been generated through the detailed parametric study and model validation efforts:

- For Lagrangian liquid spray simulations, the effervescent breakup mechanism is an essential addition to the commonly used aerodynamic breakup to account for the unique droplet–bubble interaction under flash boiling conditions.
- The effervescent breakup model features three main parameters k_{Vb}, k_b, and k_v that dictate different aspects of the flash boiling spray behavior. Detailed calibration of these model parameters is essential and achievable through near-field liquid density map matching against X-ray measurements. The calibration has been demonstrated effective for predicting near- and far-field spray morphology over the applicable range of flash boiling conditions.
- It is crucial to account for realistic fuel properties, especially liquid volatility, in order to properly predict fuel spray behavior at flash boiling conditions. Simple single-component surrogate is *not* recommended for these analysis.
- The methodology for simulating and validating Lagrangian spray simulations against X-ray experiments were established in this study. Specific meshing strategies should be applied, and proper post-processing techniques are essential for fair comparisons between numerical and experiment results.

CRediT authorship contribution statement

Francesco Duronio: Writing – original draft, Visualization, Validation, Software, Methodology, Investigation, Formal analysis, Conceptualization. **Anqi Zhang:** Writing – review & editing, Resources, Conceptualization. **Le Zhao:** Writing – review & editing, Resources, Conceptualization. **Angelo De Vita:** Supervision, Resources.

Declaration of competing interest

The authors declare that they have no known competing financial interests or personal relationships that could have appeared to influence the work reported in this paper.

Acknowledgments

This work has been funded by the European Union - NextGenerationEU, Mission 4, Component 1, under the Italian Ministry of University and Research (MUR) National Innovation Ecosystem grant ECS00000041 - VITALITY - CUP E13C22001060006.

The CFD simulations were performed on the CINECA's Galileo100 cluster within the agreement between DIIIE—Università degli Studi dell'Aquila and CINECA.

The authors wish to thank Professor Tommaso Lucchini for the invaluable initial discussions that led to the definition of the class of breakup models ruled by thermodynamic mechanisms as effervescent breakup models.

Data availability

Data will be made available on request.

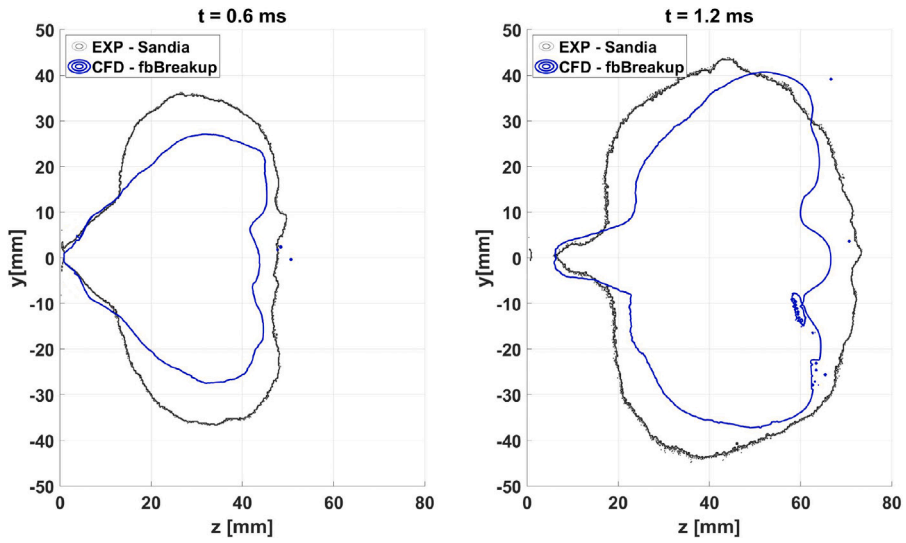

Fig. 20. Numerical and experimental [40] spray morphology represented by liquid boundary identified by a PLV threshold of $2.0 \cdot 10^{-4}$ $mm^3\,mm^{-2}$. (For interpretation of the references to color in this figure legend, the reader is referred to the web version of this article.)

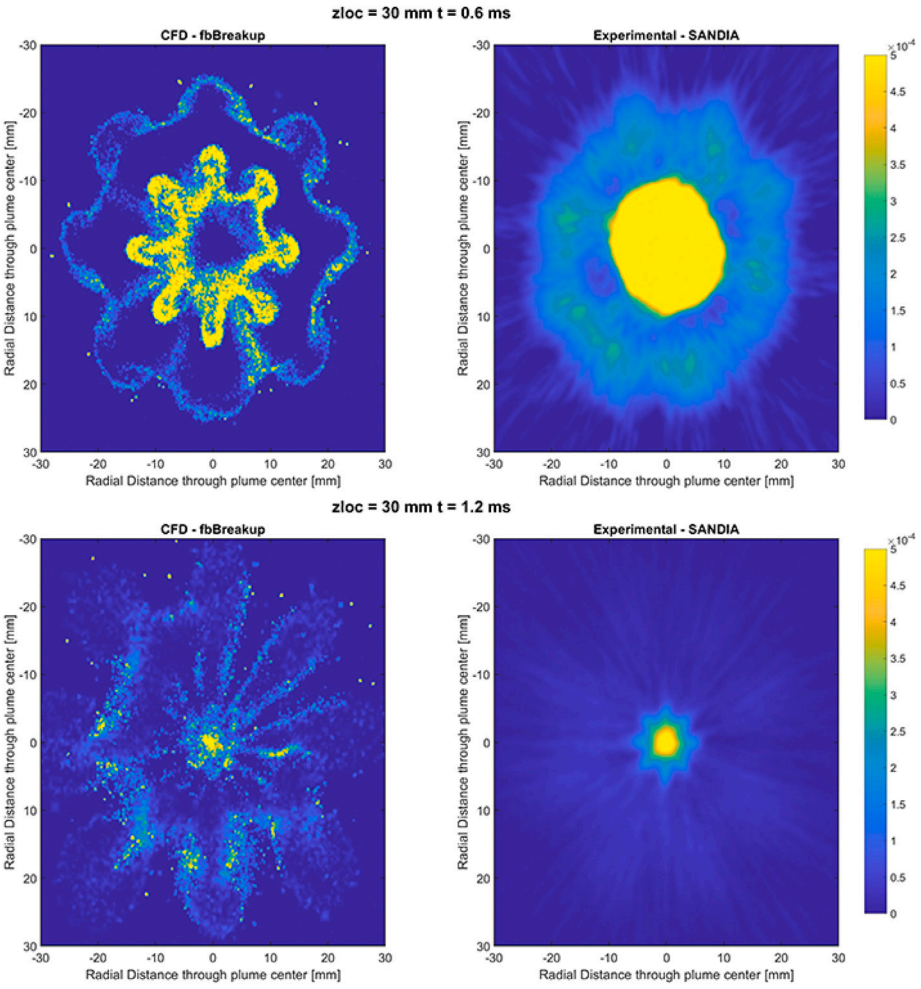

Fig. 21. LVF plotted on axial cross-section at 30 mm from the injector tip. The units are $mm^3\,mm^{-3}$.

References

[1] A. Pandal, J. Zembi, M. Battistoni, C. Hespel, R. Pele, P. Brequigny, C. Rousselle, Gdi ammonia spray numerical simulation by means of openfoam, in: WCX SAE World Congress Experience, SAE International, 2023, http://dx.doi.org/10.4271/2023-01-0311.

[2] F. Ramognino, L. Sforza, T. Cerri, T. Lucchini, A. Onorati, R. Novella, A fast and reliable cfd approach to design hydrogen si engines for industrial applications, in: 23rd Stuttgart International Symposium, SAE International, 2023, http://dx.

doi.org/10.4271/2023-01-1208.

[3] H. Guo, Y. Li, H. Xu, S. Shuai, H. Zhang, Interaction between under-expanded flashing jets: A numerical study, Int. J. Heat Mass Transfer 137 (2019) 990–1000, http://dx.doi.org/10.1016/j.ijheatmasstransfer.2019.04.010.

[4] F. Duronio, A. De Vita, A. Montanaro, C. Villante, Gasoline direct injection engines – a review of latest technologies and trends. part 2, 2020, http://dx.doi.org/10.1016/j.fuel.2019.116947, URL https://www.sciencedirect.com/science/article/pii/S0016236119323403.

[5] M. Xu, Y. Zhang, W. Zeng, G. Zhang, M. Zhang, Flash boiling: Easy and better way to generate ideal sprays than the high injection pressure, SAE Int. J. Fuels Lubr. 6 (1) (2013) 137–148, http://dx.doi.org/10.4271/2013-01-1614.

[6] E. Sher, T. Bar-Kohany, A. Rashkovan, Flash-boiling atomization, Prog. Energy Combust. Sci. 34 (4) (2008) 417–439, http://dx.doi.org/10.1016/j.pecs.2007.05.001, URL https://www.sciencedirect.com/science/article/pii/S0360128507000500.

[7] T. Bar-Kohany, E. Sher, Flash boiling atomization under negative pressure conditions, At. Sprays 31 (8) (2021) 1–8.

[8] A.H. Lefebvre, V.G. McDonell, Atomization and Sprays, CRC Press, 2017.

[9] E. Brennen, Cavitation and Bubble Dynamics Christopher, California Institute of Technology Pasadena, California-New York, 1995.

[10] H. Guo, H. Ding, Y. Li, X. Ma, Z. Wang, H. Xu, J. Wang, Comparison of spray collapses at elevated ambient pressure and flash boiling conditions using multi-hole gasoline direct injector, Fuel (2017) http://dx.doi.org/10.1016/j.fuel.2017.02.071.

[11] Y. Li, H. Guo, S. Fei, X. Ma, Z. Zhang, L. Chen, L. Feng, Z. Wang, An exploration on collapse mechanism of multi-jet flash-boiling sprays, Appl. Therm. Eng. (2018) http://dx.doi.org/10.1016/j.applthermaleng.2018.01.102.

[12] H. Guo, L. Nocivelli, R. Torelli, S. Som, Towards understanding the development and characteristics of under-expanded flash boiling jets, Int. J. Multiph. Flow 129 (2020) 103315, http://dx.doi.org/10.1016/j.ijmultiphaseflow.2020.103315, URL https://www.sciencedirect.com/science/article/pii/S0301932219309693.

[13] H. Guo, L. Nocivelli, R. Torelli, Numerical study on spray collapse process of ecn spray g injector under flash boiling conditions, Fuel 290 (2021) 119961, http://dx.doi.org/10.1016/j.fuel.2020.119961, URL https://www.sciencedirect.com/science/article/pii/S0016236120329574.

[14] F. Duronio, S. Ranieri, A. Montanaro, L. Allocca, A. De Vita, ECN Spray G injector: Numerical modelling of flash-boiling breakup and spray collapse, Int. J. Multiph. Flow 145 (2021) 103817, http://dx.doi.org/10.1016/j.ijmultiphaseflow.2021.103817, URL https://linkinghub.elsevier.com/retrieve/pii/S0301932221002470.

[15] F. Duronio, A. De Vita, A. Montanaro, L. Allocca, Experimental investigation and numerical cfd assessment of a thermodynamic breakup model for superheated sprays with injection pressure up to 700 bar, Fluids 8 (5) (2023) http://dx.doi.org/10.3390/fluids8050155, URL https://www.mdpi.com/2311-5521/8/5/155.

[16] M. Migliaccio, A. Montanaro, D. Paredi, T. Lucchini, L. Allocca, G. D'Errico, CFD Modeling and Validation of the ECN Spray G Experiment under a Wide Range of Operating Conditions, SAE Technical Papers, 2019, http://dx.doi.org/10.4271/2019-24-0130.

[17] F. Duronio, A. De Vita, A. Montanaro, C. Villante, Gasoline direct injection engines - A review of latest technologies and trends. Part 2, 2020, http://dx.doi.org/10.1016/j.fuel.2019.116947.

[18] F. Duronio, A.D. Mascio, C. Villante, M. Anatone, A.D. Vita, Ecn spray g: Coupled eulerian internal nozzle flow and lagrangian spray simulation in flash boiling conditions, Int. J. Engine Res. 14680874221090732, http://dx.doi.org/10.1177/14680874221090732.

[19] L. Qian, J. Lin, Modeling on effervescent atomization: A review, Sci. China Phys. Mech. Astron. 54 (2011) 2109–2129, http://dx.doi.org/10.1007/s11433-011-4536-1.

[20] D. Konstantinov, R. Marsh, P.J. Bowen, A. Crayford, Effervescent atomization for industrial energy technology review, At. Sprays 20 (6) (2010) 525–552.

[21] S. Sovani, P. Sojka, A. Lefebvre, Effervescent atomization, Prog. Energy Combust. Sci. 27 (4) (2001) 483–521, http://dx.doi.org/10.1016/S0360-1285(00)00029-0, URL https://www.sciencedirect.com/science/article/pii/S0360128500000290.

[22] W. Zeng, M. Xu, G. Zhang, Y. Zhang, D.J. Cleary, Atomization and vaporization for flash-boiling multi-hole sprays with alcohol fuels, Fuel 95 (2012) 287–297, http://dx.doi.org/10.1016/j.fuel.2011.08.048, URL https://linkinghub.elsevier.com/retrieve/pii/S0016236111005229.

[23] M. Lü, Z. Ning, K. Yan, J. Fu, Y. Song, C. Sun, Breakup of cavitation bubbles within the diesel droplet, Chin. J. Mech. Eng. 27 (2014) 198–204, http://dx.doi.org/10.3901/CJME.2014.01.198.

[24] E. Sher, C. Elata, Spray formation from pressure cans by flashing, Ind. Eng. Chem. Process Des. Dev. 16 (1977) 237–242, http://dx.doi.org/10.1021/i260062a014.

[25] J. Senda, Y. Hojyo, H. Fujimoto, Modeling on atomization and vaporization process in flash boiling spray, JSAE Rev. 15 (4) (1994) 291–296, URL https://www.sciencedirect.com/science/article/pii/0389430494902097.

[26] M. Razzaghi, Droplet size estimation of two-phase flashing jets, Nucl. Eng. Des. 114 (1) (1989) 115–124, http://dx.doi.org/10.1016/0029-5493(89)90130-1, URL https://www.sciencedirect.com/science/article/pii/0029549389901301.

[27] H. Guo, Y. Li, B. Wang, H. Zhang, H. Xu, Numerical investigation on flashing jet behaviors of single-hole GDI injector, Int. J. Heat Mass Transfer 130 (2019) 50–59, http://dx.doi.org/10.1016/j.ijheatmasstransfer.2018.10.088, URL https://linkinghub.elsevier.com/retrieve/pii/S0017931018326164.

[28] J.W. Gartner, Y. Feng, A. Kronenburg, O.T. Stein, Numerical investigation of spray collapse in gdi with openfoam, Fluids 6 (3) (2021) http://dx.doi.org/10.3390/fluids6030104, URL https://www.mdpi.com/2311-5521/6/3/104.

[29] X. Xi, H. Liu, M. Jia, M. Xie, H. Yin, A new flash boiling model for single droplet, Int. J. Heat Mass Transfer 107 (2017) 1129–1137, http://dx.doi.org/10.1016/j.ijheatmasstransfer.2016.11.027, URL https://www.sciencedirect.com/science/article/pii/S0017931016321469.

[30] C. Price, A. Hamzehloo, P. Aleiferis, D. Richardson, An approach to modeling flash-boiling fuel sprays for direct-injection spark-ignition engines, At. Sprays 26 (12) (2016) 1197–1239, http://dx.doi.org/10.1615/AtomizSpr.2016015807.

[31] C. Price, A. Hamzehloo, P. Aleiferis, D. Richardson, Numerical modelling of fuel spray formation and collapse from multi-hole injectors under flash-boiling conditions, Fuel (2018) http://dx.doi.org/10.1016/j.fuel.2018.01.088.

[32] S. Yang, X. Li, D.L. Hung, M. Xu, Characteristics and correlation of nozzle internal flow and jet breakup under flash boiling conditions, Int. J. Heat Mass Transfer 127 (2018) 959–969, http://dx.doi.org/10.1016/j.ijheatmasstransfer.2018.07.109, URL https://www.sciencedirect.com/science/article/pii/S0017931018316478.

[33] S. Wu, M. Xu, D.L. Hung, H. Pan, Effects of nozzle configuration on internal flow and primary jet breakup of flash boiling fuel sprays, Int. J. Heat Mass Transfer 110 (2017) 730–738, http://dx.doi.org/10.1016/j.ijheatmasstransfer.2017.03.073, URL https://www.sciencedirect.com/science/article/pii/S0017931016328605.

[34] Z. Wang, X. Dai, F. Liu, Z. Li, H. Wu, Breakup of fuel sprays under cavitating and flash boiling conditions, Appl. Therm. Eng. 143 (2018) 22–33, http://dx.doi.org/10.1016/j.applthermaleng.2018.07.090, URL https://www.sciencedirect.com/science/article/pii/S135943111832800X.

[35] G. Stiesch, Modeling Engine Spray and Combustion Processes, Springer Science & Business Media, 2003.

[36] D. Paredi, T. Lucchini, G. D'Errico, A. Onorati, L. Pickett, J. Lacey, Validation of a comprehensive computational fluid dynamics methodology to predict the direct injection process of gasoline sprays using Spray G experimental data, Int. J. Engine Res. (2020) http://dx.doi.org/10.1177/1468087419868020.

[37] G. Faeth, Current status of droplet and liquid combustion, Prog. Energy Combust. Sci. 3 (4) (1977) 191–224, http://dx.doi.org/10.1016/0360-1285(77)90012-0, URL https://www.sciencedirect.com/science/article/pii/0360128577900120.

[38] K. Richards, P. Senecal, E. Pomraning, Converge 3.0, convergent science, Madison, wi, usa, 2021.

[39] A.A. Amsden, P.J. O'Rourke, T.D. Butler, Kiva-ii: A computer program for chemically reactive flows with sprays, 1989, http://dx.doi.org/10.2172/6228444, URL https://www.osti.gov/biblio/6228444.

[40] E.C. Network, 2020, https://ecn.sandia.gov/.

[41] F. Duronio, S. Ranieri, A. Montanaro, L. Allocca, A. De Vita, Ecn spray g injector: Numerical modelling of flash-boiling breakup and spray collapse, Int. J. Multiph. Flow 145 (2021) 103817, http://dx.doi.org/10.1016/j.ijmultiphaseflow.2021.103817.

[42] Y. Zeng, Modelling of Multicomponent Fuel Vaporization in Internal Combustion Engines (Ph.D. thesis), 2000.

[43] Z. Bilicki, J. Kestin, J.T. Stuart, Physical aspects of the relaxation model in two-phase flow, Proc. R. Soc. A 428 (1875) (1990) 379–397, http://dx.doi.org/10.1098/rspa.1990.0040.

[44] R. Reitz, Modeling atomization processes in high-pressure vaporizing sprays, At. Spray Technol. 3 (1987) 309–337.

[45] Comparison Between a Center-Mounted and a Side-Mounted Injector for Gasoline Applications: A Computational Study, Vol. ASME 2020 Internal Combustion Engine Division Fall Technical Conference of Internal Combustion Engine Division Fall Technical Conference, http://dx.doi.org/10.1115/ICEF2020-2991.

[46] L. Di Angelo, F. Duronio, A. De Vita, A. Di Mascio, Cartesian mesh generation with local refinement for immersed boundary approaches, J. Mar. Sci. Eng. 9 (6) (2021) http://dx.doi.org/10.3390/jmse9060572.

[47] P.K. Senecal, E. Pomraning, K.J. Richards, S. Som, Grid-convergent spray models for internal combustion engine computational fluid dynamics simulations, J. Energy Resour. Technol. 136 (1) (2013) 012204, http://dx.doi.org/10.1115/1.4024861, arXiv:https://asmedigitalcollection.asme.org/energyresources/article-pdf/136/1/012204/6144976/jert_136_01_012204.pdf.

[48] B.A. Sforzo, A. Tekawade, A.L. Kastengren, K. Fezzaa, J. Ilavsky, C.F. Powell, Y. Pei, A. Zhang, R. Levy, X-ray characterization of real fuel sprays for gasoline direct injection, J. Energy Resour. Technol. 144 (2) (2021) 022303, http://dx.doi.org/10.1115/1.4050979.

[49] M. Cordier, L. Itani, G. Bruneaux, Quantitative measurements of preferential evaporation effects of multicomponent gasoline fuel sprays at ECN Spray G conditions, Int. J. Engine Res. 21 (1) (2020) 185–198, http://dx.doi.org/10.1177/1468087419838391.

[50] M. Bardi, A. Di Lella, G. Bruneaux, A novel approach for quantitative measurements of preferential evaporation of fuel by means of two-tracer laser induced fluorescence, Fuel 239 (2019) 521–533, http://dx.doi.org/10.1016/j.fuel.2018.11.039.